

Raman Generation by Phased and Antiphased Molecular States

A. V. Sokolov, D. R. Walker, D. D. Yavuz, G. Y. Yin, and S. E. Harris

Edward L. Ginzton Laboratory, Stanford University, Stanford, California 94305

(Received 14 December 1999)

We use molecular deuterium and two driving lasers to demonstrate collinear generation of mutually coherent equidistant sidebands, covering $50\,000\text{ cm}^{-1}$ of spectral bandwidth and ranging from $2.94\text{ }\mu\text{m}$ to 195 nm in wavelength. The essential idea is the adiabatic preparation of a single, highly coherent ($|\rho_{ab}| = 0.33$) molecular eigenstate.

PACS numbers: 42.50.Gy, 32.80.Qk, 42.60.Fc, 42.65.Dr

It has recently been predicted that coherent molecular oscillations can produce laser frequency modulation (FM), with a total bandwidth extending over the infrared, visible, and ultraviolet spectral regions, and with a possibility of subfemtosecond pulse compression. The essence of this technique is the use of a Raman transition with a sufficiently large coherence that the generation length and the phase-slip length are of the same order. This coherence is established by driving the molecular transition with two single-mode laser fields, slightly detuned from the Raman resonance so as to excite a single molecular eigenstate. Molecular motion, either in phase with the driving force (Raman detuning below resonance) or antiphased (detuning above resonance), in turn modulates the driving laser frequencies, causing the collinear generation of a very broad FM-like spectrum [1].

This Letter describes the first experimental results for this technique. Using molecular deuterium (D_2), we demonstrate collinear generation of a Raman spectrum extending over $50\,000\text{ cm}^{-1}$. The spectrum consists of seventeen mutually coherent sidebands, spaced by the fundamental vibrational frequency of D_2 (2994 cm^{-1}), and ranging in wavelength from $2.94\text{ }\mu\text{m}$ to 195 nm .

There is prior work on broadband coherent Raman generation. Several groups have studied the enhancement of stimulated Raman scattering by application of the first Stokes component collinearly with the pump laser beam; they have demonstrated increased conversion efficiency, improved reproducibility, and small divergence of the anti-Stokes beams [2–4]. Hakuta *et al.* have demonstrated collinear Raman sideband generation in solid molecular hydrogen (H_2) [5]. Nazarkin *et al.* have shown efficient laser frequency modulation by impulsively exciting a coherent vibration of SF_6 [6]. In other experiments, Ruhman *et al.* have used impulsive stimulated Raman scattering to observe coherent molecular vibrations in the time domain [7]. The phased and antiphased excitation techniques, and the resultant maximum coherence of a molecular state, have not been discussed.

Our experimental setup is shown in Fig. 1. We use two transform-limited laser pulses at wavelengths of $1.0645\text{ }\mu\text{m}$ and 807.22 nm , such that the (tunable) laser-frequency difference is approximately equal to the fundamental vibrational frequency in D_2 . The first laser is

a Quanta-Ray GCR-290 Q -switched injection-seeded Nd:YAG laser. Its output is attenuated to produce 100 mJ , 12 ns transform-limited pulses at a 10 Hz repetition rate. The laser linewidth is calculated to be $\delta\omega_{\text{laser}} = 37\text{ MHz}$. The second laser is a lab-built Ti:sapphire system, injection seeded from an external-cavity laser diode and pumped by the second harmonic of a separate Q -switched Nd:YAG laser. This laser produces 75 mJ , 16 ns transform-limited pulses at the seeding laser wavelength. This wavelength can be tuned precisely and is monitored by a Burleigh WA-1500 Wavemeter (resolution of 50 MHz). The two driving laser pulses are synchronized by adjusting the delay between the two Nd:YAG laser Q -switch trigger pulses. The laser beams are combined on a dichroic beam splitter and are loosely focused to a nearly diffraction-limited spot in a D_2 cell. The $1.06\text{ }\mu\text{m}$ laser spot size is $460\text{ }\mu\text{m}$, and the 807 nm laser spot size is $395\text{ }\mu\text{m}$.

We determine the Raman resonance by scanning the Ti:sapphire laser frequency and measuring weak Stokes gain at a low pump intensity and a small D_2 density. The D_2 cell is cooled by liquid nitrogen to $T = 77\text{ K}$; the length of the cooled region is 50 cm . Cooling reduces the Doppler linewidth to 260 MHz and increases the population of the ground rotational state of D_2 to 60% .

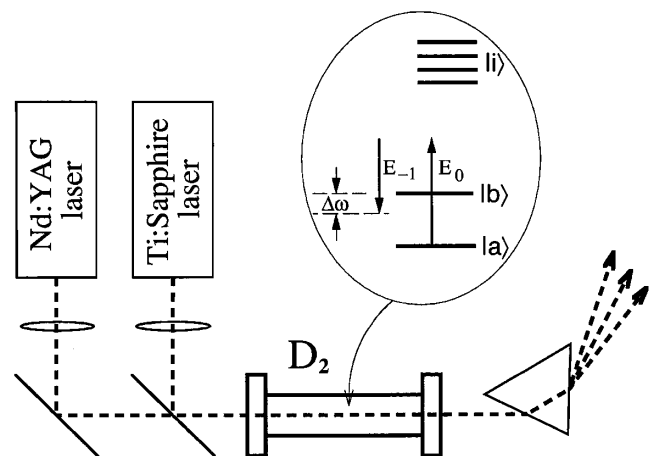


FIG. 1. Experimental setup and energy level diagram for coherent molecular excitation and collinear Raman generation. The Raman detuning $\Delta\omega$ (positive as shown) is set by the driving laser frequencies.

The collisional dephasing linewidth in D_2 at $T = 77$ K is 450 kHz/torr, as deduced from room-temperature data [8].

When we tune the driving infrared lasers to within 1 GHz from the Raman resonance, we see a bright beam of white light at the output of the D_2 cell. We disperse the spectrum with a prism and project (without collimating or focusing) onto a white scintillating screen (60 cm wide, 270 cm away from the cell). At a D_2 pressure of 50–100 torr and at a Raman detuning of a few hundred MHz, we observe up to thirteen anti-Stokes sidebands and two Stokes sidebands, in addition to the two driving frequencies. These sidebands are spaced by 2994 cm^{-1} and range from $2.94\text{ }\mu\text{m}$ to 195 nm in wavelength. The next Stokes sideband has a wavelength of $24\text{ }\mu\text{m}$ and is difficult to detect. The next (fourteenth) anti-Stokes sideband has a wavelength of 184 nm and is absorbed by air.

Figure 2 shows pictures of the spectrum taken with a digital color camera with a single-shot exposure at a fixed aperture size. Starting from the left, the first two sidebands are the driving frequencies, and the next four are anti-Stokes sidebands in real color (red, green, blue, and violet); beginning at the fifth anti-Stokes, the sidebands are in the ultraviolet and only fluorescence is visible. Figures 2(a)–2(c) show the spectrum generated at a D_2 pressure of $P = 71$ torr and a Raman detuning of $\Delta\omega = -400 \pm 25$ MHz in part (a), $\Delta\omega = 100 \pm 25$ MHz in part (b), and $\Delta\omega = 700 \pm 25$ MHz in part (c). The smooth near-Gaussian beam profiles for nearly all sidebands, as shown in Figs. 2(a)–2(c), demonstrate collinear anti-Stokes generation in a regime of high molecular coherence. At higher pressures the generation is no longer collinear and the anti-Stokes sidebands emerge in circles of increasing diameter. An example at a pressure of 350 torr and $\Delta\omega = 700$ MHz is shown in Fig. 2(d).

Figure 3 shows Stokes and anti-Stokes energy spectra for three different values of the Raman detuning and contrasts the on-resonance generation at $P = 72$ torr (triangles and solid line) with the generation below resonance

(circles and dashed line) and above resonance (squares and dotted line). We observe that on-resonance generation is less efficient than off-resonance generation for all of the anti-Stokes sidebands, and that generation below resonance is more efficient than above resonance. Note that we generate hundreds of μJ per pulse (at a 10 Hz repetition rate) at sidebands far into the UV.

We now proceed with the discussion of these results. We consider a set of equidistant Raman sidebands with complex field envelopes E_q and carrier frequencies ω_q , tuned close to the Raman transition $|a\rangle \rightarrow |b\rangle$, and far detuned from the upper electronic states $|i\rangle$. Propagation of each sideband is governed by the slowly varying envelope equation in local time [1]:

$$\frac{\partial E_q}{\partial z} = -j\eta\hbar\omega_q N(a_q\rho_{aa}E_q + d_q\rho_{bb}E_q + b_q^*\rho_{ab}E_{q-1} + b_{q+1}\rho_{ab}^*E_{q+1}), \quad (1)$$

where ρ_{aa} and ρ_{bb} are populations of states $|a\rangle$ and $|b\rangle$, ρ_{ab} is the Raman coherence, N is the molecular density, and $\eta = (\mu/\epsilon_0)^{1/2}$. Expressions for the dispersion and coupling constants a_q , b_q , and d_q are given in Ref. [1].

When the magnitude of the coherence ρ_{ab} approaches its maximum value of 0.5, the coupling terms in Eq. (1) (last two terms) are of the same order as the dispersion terms (first two terms). In such a high-coherence regime, the generation length becomes comparable to the phase-slip length, and efficient generation proceeds collinearly, with phase matching playing a small role [9]. To the extent that dispersion can be neglected completely, theory predicts a pure sinusoidal frequency modulation of a laser beam, as a result of its propagation through the coherent medium [1].

The excitation of the molecular states $|a\rangle$ and $|b\rangle$ is described by an effective two-by-two Hamiltonian [1]:

$$H_{\text{eff}} = -\frac{\hbar}{2} \begin{bmatrix} A & B \\ B^* & D - 2\Delta\omega \end{bmatrix}, \quad (2)$$

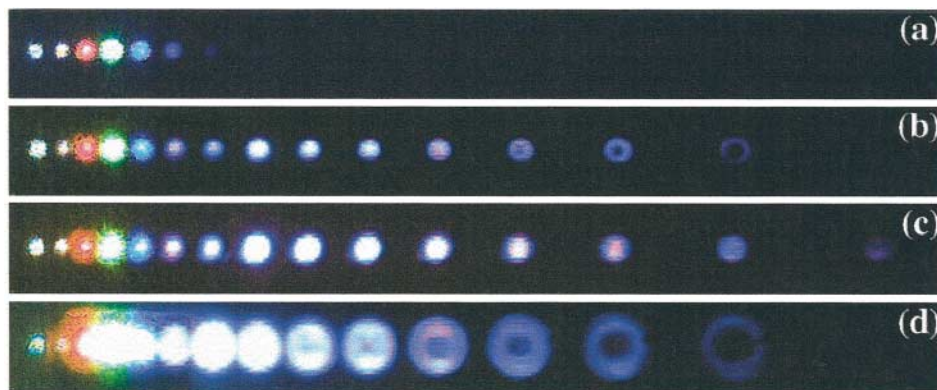


FIG. 2 (color). Spectrum generated in the setup of Fig. 1 at (a) $P = 71$ torr and $\Delta\omega = -400$ MHz, (b) $P = 71$ torr and $\Delta\omega = 100$ MHz, (c) $P = 71$ torr and $\Delta\omega = 700$ MHz, and (d) $P = 350$ torr and $\Delta\omega = 700$ MHz. We observe the two driving infrared fields (on the left), and multiple generated visible and ultraviolet anti-Stokes sidebands. To reduce camera saturation for (a)–(c), the first four anti-Stokes beams are attenuated by a factor of 100; the driving field at 807 nm and also the fifth anti-Stokes beam are attenuated by 10. In (d), the 807 nm beam and the first four anti-Stokes beams are attenuated by 10.

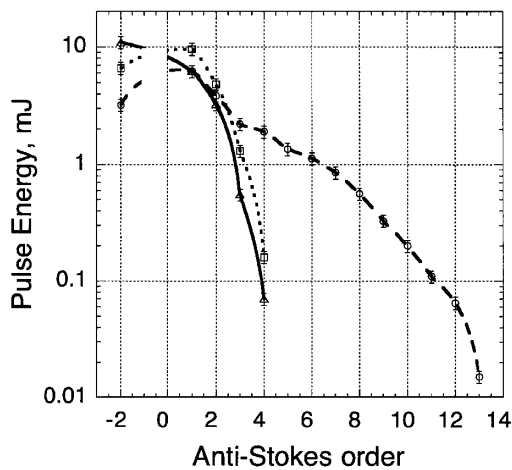


FIG. 3. Pulse energies generated in the setup of Fig. 1 at $P = 72$ torr. The triangles show on-resonance generation ($\Delta\omega = 0$), the circles show generation by phased ($\Delta\omega = 500$ MHz) and the squares by anti-phased ($\Delta\omega = -200$ MHz) states of D_2 .

where $A = \sum_q a_q |E_q|^2$, $B = \sum_q b_q E_q E_{q-1}^*$, and $D = \sum_q d_q |E_q|^2$. The Raman detuning $\Delta\omega$ is the difference between the molecular transition frequency $\omega_b - \omega_a$ and the frequency of the driving force $\omega_q - \omega_{q-1}$. The collisional dephasing is included in the equation for the off-diagonal density-matrix element (the coherence) ρ_{ab} . For the preparation of maximum coherence it is essential that the dephasing time is longer than the laser pulse length (as is the case in our experiment).

The molecular eigenstate which evolves from the ground state as the field amplitudes are increased and the coherence which is obtained from it are

$$|+\rangle = \cos\frac{\theta}{2} \exp\left(j\frac{\varphi}{2}\right)|a\rangle + \sin\frac{\theta}{2} \exp\left(-j\frac{\varphi}{2}\right)|b\rangle, \quad (3)$$

$$\rho_{ab} = \frac{1}{2} \sin\theta \exp(j\varphi),$$

where $B = |B| \exp(j\varphi)$ and $\tan\theta = 2|B|/(2\Delta\omega - D + A)$. When the Raman detuning is larger than the driving laser linewidth, the molecular system follows this eigenstate adiabatically, with the sign of ρ_{ab} determined by the sign of the Raman detuning. In a resonant, nonadiabatic regime the molecules exhibit two-photon Rabi flopping at a frequency B .

In our experiment the Doppler broadened linewidth (260 MHz) of the 2994 cm^{-1} transition of D_2 is larger than both the collisional dephasing rate (32 MHz for $P = 72$ torr) and the laser linewidth (37 MHz). When we tune close to the center of the Doppler line, we expect adiabatic preparation for most of the molecules in both wings of the velocity distribution, with significant magnitude of their excitation when the coupling parameter $B > \delta\omega_{\text{laser}}$. The phases of these excitations are positive or negative depending on the sign of the Raman detuning, such that the contributions of these molecules partially cancel each other, resulting in a smaller integrated value

of the coherence ρ_{ab} at the center frequency. However, when we detune to either side of the Doppler line, we expect adiabatic preparation of nearly all of the molecules in the same (phase or antiphased) state [Eqs. (3)], resulting in a larger total coherence and more efficient Raman generation. Similar behavior has been observed in saturated coherent anti-Stokes Raman spectroscopy [10].

Figure 4 illustrates this behavior. Parts (a) and (b) show the first anti-Stokes pulse energy as a function of the Raman detuning, both at low pressure ($P = 6$ torr). Here, the depletion of the applied fields is not important, and the generated energy is proportional to the square of the Doppler-averaged coherence [Eq. (1)]. In Fig. 4(a), the $1.06 \mu\text{m}$ laser pulse energy is 5.4 mJ and $B = 39 \text{ MHz} \approx \delta\omega_{\text{laser}}$; for these conditions the anti-Stokes generation peaks on resonance. For Fig. 4(b) we apply full power of the driving lasers, so that $B = 168 \text{ MHz} \gg \delta\omega_{\text{laser}}$, and observe that the anti-Stokes generation peaks on both sides of the resonance, with a dip exactly on resonance. The peak at positive $\Delta\omega$ is higher, because, as the laser power increases as a function of time, this peak Stark-shifts toward resonance. We solve the full density-matrix equations numerically for the experimental driving laser pulses, calculate the (complex) coherence ρ_{ab} at the pulse peak for different values of Raman detuning, and average it over the Doppler distribution. The solid lines in Figs. 4(a) and 4(b) show the square of the Doppler-averaged coherence (no scaling). We calculate that the maximal value of the coherence that we achieve in our experiment is $|\langle\rho_{ab}\rangle_{\text{Doppler}}| = 0.33$.

Figure 4(c) shows qualitatively similar behavior at a higher D_2 pressure ($P = 72$ torr). The filled circles represent the sum of all generated Stokes and anti-Stokes sidebands. The open circles and triangles show the first and second anti-Stokes sidebands. All measurements for Figs. 3 and 4 are done with a Moletron J4-09 pyroelectric detector. Each point in the plots is an average over eight laser shots, with error bars showing the standard deviation for each data set.

In order to investigate adiabatic and nonadiabatic molecular excitation we measure the total laser energy transmitted through the D_2 cell (including all applied and generated sidebands) as a function of the Raman detuning. When the molecular evolution is adiabatic, we expect all molecules to return to the ground state as the laser fields decrease at the falling edge of the applied pulses. We observe a dip in transmission on Raman resonance, confirming that energy is left in the molecular system due to nonadiabatic behavior. For comparison we numerically calculate the probability for the molecular system to remain in the adiabatic eigenstate $|+\rangle$ [Eqs. (3)], averaged over the Doppler distribution [solid line in Fig. 4(d)], again demonstrating good qualitative agreement between theory and experiment. By comparing Figs. 4(c) and 4(d), we note that the Raman generation peaks at detunings where the molecular evolution is completely adiabatic.

We note the connection of this work to the coherent population transfer [11] and to electromagnetically induced

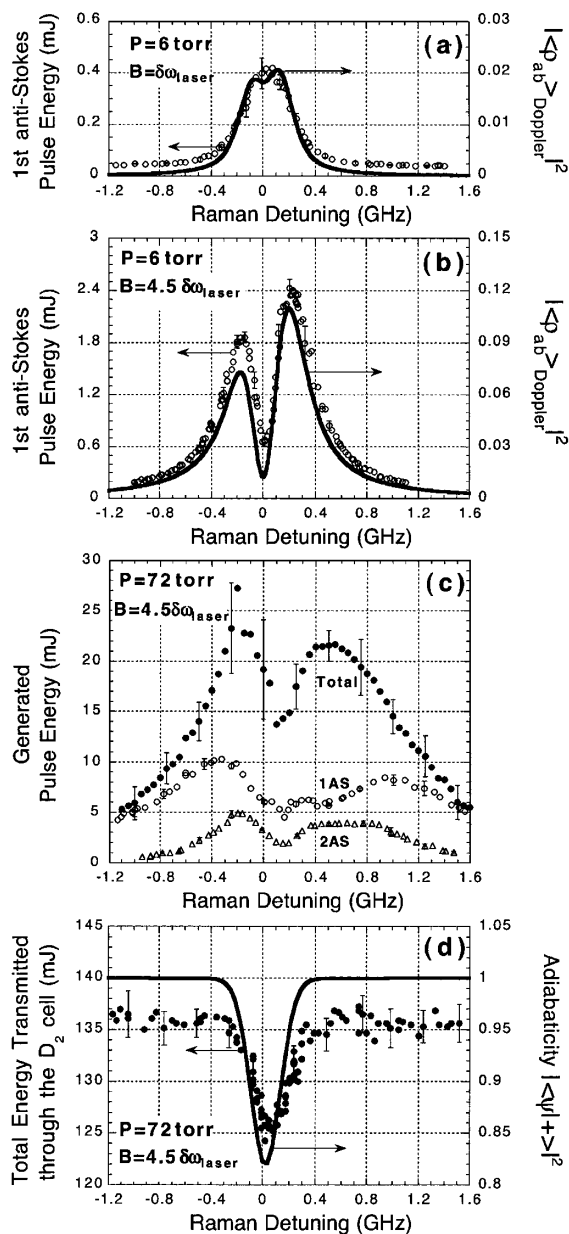


FIG. 4. Raman generation by adiabatic eigenstates in D_2 . (a) First anti-Stokes generation by weakly driven vibrations ($B \approx \delta\omega_{\text{laser}}$) at $P = 6$ torr. (b) First anti-Stokes generation by strongly driven vibrations ($B \gg \delta\omega_{\text{laser}}$) at $P = 6$ torr. In both (a) and (b) the solid lines show the calculated square of the Doppler-averaged coherence ρ_{ab} at the pulse peak. (c) Sum over pulse energies of all generated Raman sidebands (filled circles), first anti-Stokes generation (open circles), and second anti-Stokes generation (triangles) for $B \gg \delta\omega_{\text{laser}}$ and $P = 72$ torr. (d) Total energy in all applied and generated sidebands at the output of the D_2 cell. The solid line represents the calculated fraction of the molecular population in the eigenstate which evolves adiabatically from the ground state [Eq. (3)].

transparency (EIT) [12]: Each involves the preparation of the adiabatically evolving eigenstate. In three-state EIT this is done by using quantum interference or optical pumping. Here it is done by fixed or adiabatically changing detuning. Both EIT and this process require that the number of photons in the laser pulse exceed the number of

molecules in the laser path [12,13]. Both allow nonlinear optics at maximum coherence, where the role of phase matching is greatly reduced [9]. But, differing from EIT, here, the refractive indices at the various sidebands are reduced (in the antiphased case) [1] but are not equal to unity.

In summary, this Letter demonstrates broadband collinear Raman generation by adiabatically prepared phased and antiphased states in molecular deuterium. We show that, in agreement with theory, generation maximizes at a finite detuning on either side of the Raman resonance. We believe it will be possible to recombine the generated sidebands and to use spectral modification techniques [14] to synthesize specified subfemtosecond time structures in a target cell.

This work was supported by the U.S. Army Research Office, the U.S. Air Force Office of Scientific Research, and the U.S. Office of Naval Research. D.R.W. also acknowledges support from the Fannie and John Hertz Foundation.

- [1] S.E. Harris and A.V. Sokolov, Phys. Rev. A **55**, R4019 (1997); S.E. Harris and A.V. Sokolov, Phys. Rev. Lett. **81**, 2894 (1998); A.V. Sokolov, D.D. Yavuz, and S.E. Harris, Opt. Lett. **24**, 557 (1999); A.V. Sokolov, Opt. Lett. **24**, 1248 (1999).
- [2] V. Schulz-von der Gathen, T. Bornemann, V. Kornas, and H.F. Dobe, IEEE J. Quantum Electron. **26**, 739 (1990).
- [3] L.L. Losev and A.P. Lutsenko, Quantum Electron. **23**, 919 (1993); G.S. McDonald, G.H.C. New, L.L. Losev, A.P. Lutsenko, and M. Shaw, Opt. Lett. **19**, 1400 (1994).
- [4] H. Kawano, Y. Hirakawa, and T. Imasaka, IEEE J. Quantum Electron. **34**, 260 (1998).
- [5] K. Hakuta, M. Suzuki, M. Katsuragawa, and J.Z. Li, Phys. Rev. Lett. **79**, 209 (1997).
- [6] A. Nazarkin, G. Korn, M. Wittman, and T. Elsaesser, Phys. Rev. Lett. **83**, 2560 (1999).
- [7] S. Ruhman, A.G. Joly, and K.A. Nelson, IEEE J. Quantum Electron. **24**, 460 (1988).
- [8] D.A. Russel and W.B. Roh, J. Mol. Spectrosc. **124**, 240 (1987).
- [9] M. Jain, H. Xia, G.Y. Yin, A.J. Merriam, and S.E. Harris, Phys. Rev. Lett. **77**, 4326 (1996); A.J. Merriam, S.J. Sharpe, H. Xia, D. Manuszak, G.Y. Yin, and S.E. Harris, Opt. Lett. **24**, 625 (1999).
- [10] R.P. Lucht and R.L. Farrow, J. Opt. Soc. Am. B **5**, 1243 (1988).
- [11] K. Bergmann, H. Theuer, and B.W. Shore, Rev. Mod. Phys. **70**, 1003 (1998).
- [12] S.E. Harris, Phys. Today **50**, No. 7, 36 (1997); M.O. Scully and M.S. Zubairy, *Quantum Optics* (Cambridge University Press, Cambridge, England, 1997).
- [13] D.D. Yavuz, A.V. Sokolov, and S.E. Harris, Phys. Rev. Lett. **84**, 75 (2000).
- [14] C.W. Hillegas, J.X. Tull, D. Goswami, D. Strickland, and W.S. Warren, Opt. Lett. **19**, 737 (1994); A.M. Weiner, Prog. Quantum Electron. **19**, 161 (1995); T. Baumert, T. Brixner, V. Seyfried, M. Strehle, and G. Gerber, Appl. Phys. B **65**, 779 (1997).